Journal of Power Sources 182 (2008) 340–348

Contents lists available at ScienceDirect

Journal of Power Sources

journal homepage: www.elsevier.com/locate/jpowsour

Influence of silica aerogel on the properties of polyethylene oxide-based nanocomposite polymer electrolytes for lithium battery

Y.W. Chen-Yang[a,*], Y.L. Wang[a], Y.T. Chen[a], Y.K. Li[a], H.C. Chen[b], H.Y. Chiu[b]

[a] Department of Chemistry, Center for Nanotechnology and R&D Center for Membrane Technology, Chung Yuan Christian University, Chung-Li 32023, Taiwan, ROC
[b] Taiwan Textile Research Institute, Taipei County 23674, Taiwan, ROC

ARTICLE INFO

Article history:
Received 13 November 2007
Received in revised form 16 March 2008
Accepted 2 April 2008
Available online 8 April 2008

Keywords:
Composite polymer electrolyte
Silica aerogel powder
Ionic conductivity
Lithium ion transference number
Electrochemical properties

ABSTRACT

In this study, a series of nanocomposite polymer electrolytes (NCPEs) with high conductivity and lithium ion transference number, PEO/$LiClO_4$/SAP, were prepared from high molecular weight polyethylene oxide (PEO), $LiClO_4$ and low content of homemade silica aerogel powder (SAP), which had higher surface area and pore volume than the conventional silica particle. From the SEM images it was found that the SAP nanoparticles were well dispersed in the PEO polymer electrolyte matrix. The characterization and interactions in the CPEs were studied by DSC, XRD, FT-IR and ^7Li NMR analysis. The ac impedance results showed that the ionic conductivity of the CPE was significantly improved by the addition of the as-prepared SAP. The maximum ambient ionic conductivity obtained from the CPE with EO/Li = 6 and 2 wt.% of SAP (O6A2) was about threefold higher than that of the corresponding polymer electrolyte without SAP (O6). In addition, the lithium ion transference number (t^+) of O6A2 at 70 °C was as high as 0.67, which was also three times higher than that of O6 and has not been previously reported for the PEO–LiX-based polymer electrolytes.

1. Introduction

Since Wright et al. found out in 1973 that the complex of poly(ethylene oxide) (PEO) and alkaline salts have the ability of ionic conductivity [1], solid polymer electrolytes (SPEs) have drawn significant interest for the possible replacement of liquid electrolytes in secondary lithium batteries due to the advantages of SPE-based lithium batteries considering safety, weight and size [2–7]. Especially, PEO-based polymer electrolytes are the most extensively studied SPEs. The main reason in choosing this polymer as the host is that it forms more stable complexes and possesses higher ionic conductivities than any other group of solvating polymers without the addition of organic solvents [3,4]. It is also known that the maximum power obtainable in a lithium cell is related to the ionic conductivity of the electrolyte, and the maximum limiting current that can be drawn from the cell and the cycle-ability of the cell depends on the cation transference number (t^+) [2,3]. Unfortunately, the PEO-based SPEs are prone to crystallization, resulting in low ambient temperature conductivities ($<10^{-7}$ S cm^{-1}) and t^+ values (~0.2) [2]. Thus, several approaches have been applied to enhance the properties of PEO-based polymer electrolytes [4,8]. One of the most effective approaches has been the addition of inorganic fillers, such as ceramic fillers (SiO_2, Al_2O_3, and TiO_2) [4–6], layered materials (montmorillonite) [9] and mesoporous materials (SBA-15, MCM-41) [10–14,], as well as syntheses of organic/inorganic hybrid materials [15,16]. The results showed that the addition of the inorganic fillers has improved many properties of the polymer electrolytes, such as ionic conductivity, lithium ion transference number (t^+), mechanical properties, and the stability of electrolyte–electrode interface [17–19]. These improvements have been ascribed to fillers that (1) acted as the plasticizers and lowered the crystallinity of the polymer matrix [20], (2) increased ion mobility by providing additional conductive pathway due to formation of the Lewis acid–base interactions [21], and (3) increased the number of charge carriers due to enhancement of the salt dissociation [22]. Besides, compared to the non-porous particle fillers, it was found out that the corresponding porous fillers usually showed higher efficiency in the enhancement of the conductive properties in the CPEs due to the higher surface area as reported for PEO/SBA-15 [12] and the larger pores, facilitating the intercalation with the PEO chains, as studied for the PEO/SBA-15 organic–inorganic composite [8]. However, the conductivities and the t^+ values reported are still not high enough for practical application; therefore, finding a new filler to enhance both the conductivity and t^+ value of the PEO-based SPE is still an attractive topic.

Silica aerogel is a tunable and designable material, which possesses unique properties, and features [23], such as low density (0.003–0.5 g cm^{-3}), high porosity (90–99%), large surface area (>800 m^2 g^{-1}) and interconnected pores and has been employed in many applications [24]. Although these unique properties are

* Corresponding author. Tel.: +886 3 265 3317; fax: +886 3 265 3399.
E-mail address: yuiwhei@cycu.edu.tw (Y.W. Chen-Yang).

0378-7753/$ – see front matter © 2008 Elsevier B.V. All rights reserved.
doi:10.1016/j.jpowsour.2008.04.001

also anticipated to better benefit to the ionic conductivity, cation transference and other related properties of the polymer composite electrolyte for lithium battery than the conventional non-porous or mesoporous silica particles, the application of silica aerogel on the preparation of CPE has not been reported.

In this study, a series of amorphous PEO/$LiClO_4$/SAP CPEs has been prepared from PEO, $LiClO_4$ and the homemade silica aerogel powder (SAP) nanoparticles. The characterization and the properties of the CPEs have been investigated with the X-ray diffraction (XRD) patterns, FT-IR and ^{7}Li MAS NMR spectroscopies, SEM/EDS images, DSC/TGA thermograms and ac impedance measurements. Also studied were the temperature dependence of the ionic conductivities, the lithium ion transference number and the electrochemical properties of the CPEs.

2. Experimental

2.1. Materials

Polyethylene oxide (M_w 5,000,000) (PEO) and lithium perchlorate ($LiClO_4$) were obtained from Aldrich Company. 1-Methylimidazol, 1-chlorobutane, tetraethoxylsilane (TEOS), sodium tetrafluoroborate ($NaBF_4$) and acetonitrile (ACN) were obtained from ACROS Company. Formic acid was acquired from TEDIA Company. All the chemicals were used as received.

2.2. Preparation of ionic liquid

The ionic liquid used for the preparation of SAP was synthesized according to the method reported [25]. Hence, 1-chlorobutane (370 g, 4 mol) was added drop wise to a solution of 1-methylimidazole (82.0 g, 1 mol) in acetonitrile (30.0 g) at room temperature and the solution was stirred overnight. After the removal of acetonitrile, the remaining salt, 1-butyl-3-methylimidazolium chloride (BMIC) was dried at 80 °C under reduced pressure. Then 218 g (1 mol) of BMIC was added to a solution of sodium tetrafluoroborate (132 g, 1.2 mol) in acetonitrile (100 g). The solution was stirred for 2 days at room temperature. The reaction mixture was filtered and the volatile substances were removed under reduced pressure. The resulting ionic liquid product, 1-butyl-3-methylimidazolium tetrafluoroborate (BMIBF) was finally obtained by filtration and drying at 120 °C under reduced pressure.

2.3. Preparation of silica aerogel powder (SAP)

The silica aerogel monolith was prepared according to the sol–gel route reported [26,27], but using BMIBF as the template and the solvent. In a typical run, 5.8 g (28 mmol) of TEOS, 1.9 g (58 mmol) of methanol, 3.0 g (12 mmol) of BMIBF and 3.4 g (189 mmol) of water were mixed together in a bottle. A monolithic gel was formed by gelation at room temperature within 3 h after mixing and cured at ambient temperature for 5 days in an open air. Then the entrapped ionic liquid was Soxhlet extracted with ethanol for 1 day. Finally, the as-prepared silica aerogel monolith was obtained by drying in a freeze drier. In order to get good dispersion, the as-prepared silica aerogel monolith was ground by a hand mill into a powder form and further mechanically ground in water with the agitator mill into a nano-sized particle form, named silica aerogel powder (SAP).

2.4. Preparation of the CPEs

For preparation of each CPE, 0.2 g of PEO was dissolved in a small amount of ACN. The required quantity of $LiClO_4$ was then added and stirred well. The desired amount of the SAP nanoparticles, according to the composition designed, was added and the solution was further stirred continuously for 24 h. The mixture was cast on a Teflon dish and evaporated under vacuum at a proper temperature to remove the solvent for at least 24 h. The dried samples were stored in an argon-filled dry box to prevent from absorbing moisture. In this study, the samples were denoted as O*x*A*y*, where *x* represents the EO/Li molar ratio and *y* represents the wt.% of SAP loaded.

2.5. Instruments

The BET specific surface area and the pore volume of the as-prepared aerogel monolith were determined from the nitrogen adsorption/desorption isotherm by the Barrett–Joyner–Halenda (BJH) method using a Micromeritics ASAP 2020 analyzer. The as-prepared silica aerogel was ground into nano-sized particles with an agitator mill (NEZSCH MiNI Cell agitator). The particle size of the ground silica aerogel powder (SAP) was measured with BTC 901 Plus. The surface morphologies of the CPEs prepared were studied using a scanning electron microscopy–energy dispersive spectroscopy (SEM/EDS) using a Hitachi 3500N–Noran Vantage DI instrument. Differential scanning calorimetry (DSC) and thermogravimetric analysis (TGA) were implemented with a Seiko DSC 220C and a Seiko TG/DTA 220, respectively. The samples were heated at a rate of 10 °C/min under a nitrogen flow from −80 to 150 °C for DSC measurement and from 30 to 200 °C for TGA measurement. Fourier transform infrared (FT-IR) spectra were recorded on a Bio-Rad FTS-7. The resolution and scan numbers of IR measurement were 2 cm^{-1} and 64 times, respectively. The spectra were collected over the range 400–4000 cm^{-1}. The XRD patterns of the samples were recorded using a PANalytical PW3040/60X'Pert pro at 45 kV and 40 mA with a step size of 0.1° and 128 ms per step. ^{7}Li MAS NMR measurement was performed on a Brucker DSX-400 spectrometer, operating at a frequency of 116.6 MHz and a spinning speed of 2 kHz. The ionic conductivities of the polymer electrolytes were measured by the complex impedance method in the temperature range of 30–80 °C. The samples were sandwiched between the stainless steel blocking electrodes and placed in a temperature-controlled oven at vacuum for 2 h before measurement. The ac impedance measurements were carried out on a computer-interfaced HP 4192A impedance analyzer over the frequency range of 5 Hz to 13 MHz. The lithium ion transference number (t^+) was measured using the technique reported [28,29]. The electrochemical cell comprised a rectangular piece of polymer electrolyte sandwiched between two lithium foils. The electrolyte was sandwiched between two lithium-unblocking electrodes to form a symmetrical Li/electrolyte/Li cell used for a t^+ test. The cell was assembled and sealed in an argon-filled UNILAB glove-box. The impedance of the cell was measured using an Autolab PGSTAT 30 potentiostat/galvanostat analyzer between the frequencies of 5 Hz and 1 MHz. The method consisted of the measurement of the initial lithium interfacial resistance (R_0) with impedance spectroscopy in the frequency range of 1 MHz to 5 Hz, the application of a small voltage (0.1 V) until a steady current was obtained (I_s), and the measurement of the final interfacial resistance (R_f) in the same frequency range. The measurements were performed using a Solartron 1260 impedance/gain-phase analyzer coupled with a Solartron 1287 electrochemical interface.

3. Results and discussion

3.1. Characterization of the silica aerogel

In order to obtain a high surface area and high pore volume silica, a silica aerogel was synthesized by the sol–gel polymer-

ization. Since the conventional supercritical drying process, used for preparation of silica aerogel, usually operates under a harsh condition, high temperature and high pressure, the sol–gel polymerization with BMIBF, an ionic liquid, as the solvent and the template was used in this study to avoid the harsh condition. This is because the unique properties of ionic liquid, including the negligible vapor pressure and ionicity, allow the hydrolysis and condensation of the sol–gel polymerization to produce a stable gel network without largely shrinking and can keep the aerogel structure after the solvent extraction and the drying process [30,31].

From the FT-IR spectra (not shown) of the as-prepared silica aerogel and the ionic liquid, the characteristic bands of silica are observed at 3700 cm^{-1} and ~3200 cm^{-1} for the ≡Si–OH vibration, 1088 cm^{-1} for the Si–O–Si asymmetric stretching vibration, and 1000–1200, 780–820 and 430–460 cm^{-1} for the ≡Si–O–Si≡ strain vibration, respectively. Besides, the disappearance of the characteristic bands of the ionic liquid, peaked at 1467 and 1720 cm^{-1}, confirmed that almost all of the ionic liquid was removed by the extraction process.

Solid-state ^{29}Si MAS NMR spectroscopy allows an investigation of the chemical environment of the ^{29}Si atom. According to the literature [32], the resonances of the different species in silica are located between −90 and −120 ppm. Q^n terminology, which denotes the silicon with n Si–O–Si linkages, is used in the ^{29}Si solid-state NMR results. The chemical shifts (relative to tetramethylsilane) of Q^n are about −80, −90, −100, and −110 ppm for Q^1, Q^2, Q^3 and Q^4, respectively. The relative proportion of the different species can be calculated by the corresponding peak area of the absorption. As can be seen in Fig. 1, Q^0 to Q^2 are not found in the as-prepared silica aerogel sample, and higher content of Q^4 species (−111.5 ppm, 78.4%) than that of Q^3 species (−101.9 ppm, 21.6%) is observed. This indicates that about 94.6% of the silanol groups were condensed during the sol–gel-ageing process.

The BET surface area and pore volume of the silica aerogel monolith were evaluated from their nitrogen adsorption/desorption isotherms with Barrett–Joyner–Halenda (BJH) method (Fig. 2). As can be seen, the isotherm is of type IV based on the Burnauer, Deming, Deming and Teller (BDDT) classification [33]. The gas adsorption occurred in the micropores at very low pressure, followed by adsorption in the mesopores, with capillary condensation occurring at the higher pressures, leading to the hysteresis loops [34]. This suggests that the as-prepared silica aerogel was a typical mesoporous material. The specific surface area (S_{Bet}) measured from the isotherm was 812 (±32.3) $m^2\,g^{-1}$, which is higher than the value of the non-porous silica particle (e.g. about 380 $m^2\,g^{-1}$ for the silica powder product of Degussa, A3802). Besides, the pore volume (V_p) obtained was as high as 1.97(±0.3) $cm^3\,g^{-1}$, which is much higher than the conventional mesoporous silica (<1.2 $cm^3\,g^{-1}$) [35], supporting that the aerogel network was not collapsed by the drying process. The high values of S_{Bet} and V_p assured the as-prepared silica aerogel good filler for CPE.

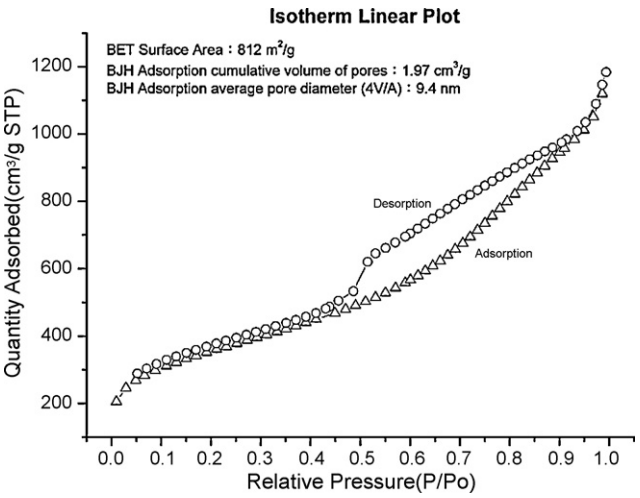

Fig. 2. The nitrogen adsorption/desorption isotherm of the silica aerogel.

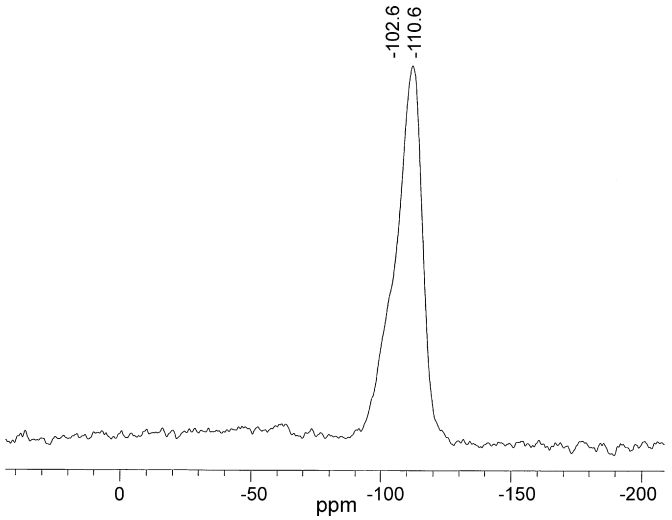

Fig. 1. ^{29}Si solid-state NMR of the silica aerogel.

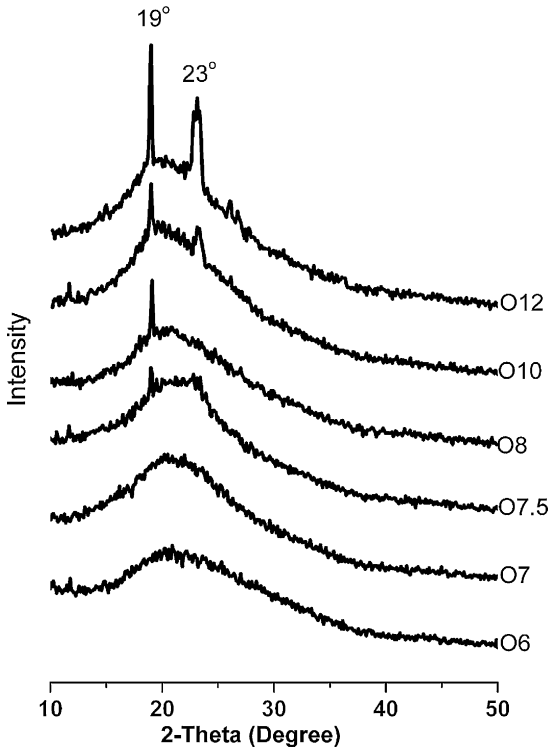

Fig. 3. Wide-angle X-ray diffraction patterns of O*x* electrolyte series.

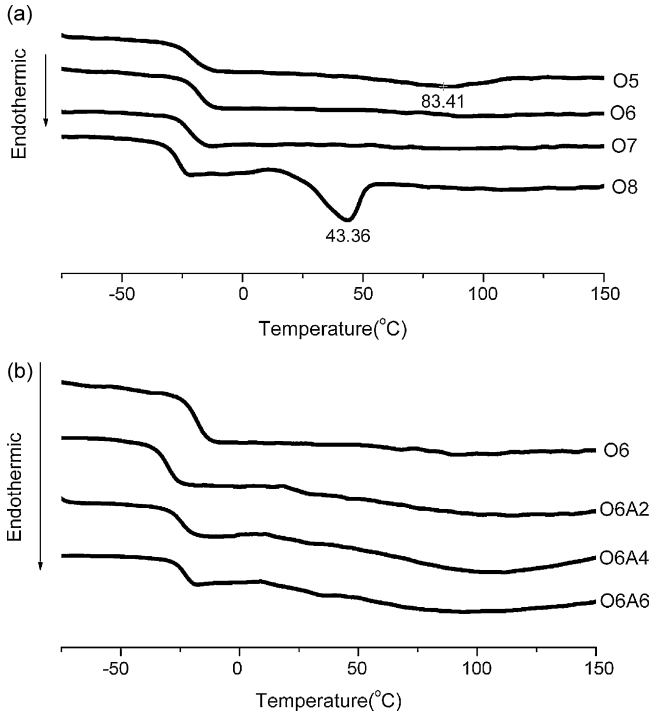

Fig. 4. DSC curves of (a) O*x* and (b) O6A*y*.

3.2. The crystallinity and morphology of the as-prepared polymer electrolytes

As is known, the degree of crystallinity of PEO-based SPE varies with concentration of the lithium salt and molecular weight of the PEO used. In order to find the best composition to reduce the crystallinity and compare with the as-prepared CPEs, a series of PEO/$LiClO_4$ SPEs with various EO/Li values (4–8) were prepared and abbreviated as O*x* (*x* = EO/Li molar ratio). It was found out that the as-prepared SPE membranes, O*x*, with EO/Li ≤ 8 were transparent or opaque and mechanically strong enough. But, when the salt content was higher (EO/Li > 8) the membranes became transparent and brittle. As shown in the XRD patterns (Fig. 3), the characteristic diffraction peaks of PEO crystalline are observed at $2\theta = 19^\circ$ and 23°. However, these peaks became weaker as the content of $LiClO_4$ was increased and no peak was found for O7 and O6. This reveals that the amorphous structure was obtained from the PEO-based polymer electrolytes with EO/Li = 6 and 7.

The DSC curves of O*x* are displayed in Fig. 4(a) and the corresponding data are summarized in Table 1. It shows that the crystallinity of the PEO (X_c) and the melting temperature (T_m) decreased as the $LiClO_4$ content was increased. However, no endothermic peak was found for O7 and O6, indicating that the crystallization was completely depressed in these SPEs as indicated by the XRD patterns. Besides, the glass transition temperature (T_g) increased with increasing the $LiClO_4$ content, indicating an increase of the interaction between Li^+ and ether oxygen and the formation of cross-linking complex as found in the other reports [18,36]. The highest T_g was obtained from O6 (EO/Li = 6), providing the best dimensional stability. The result implies that the polymer electrolyte O6 would show the highest conductivity in the O*x* system. Besides, in order to obtain the one with the highest conductivity and lithium transference number in the PEO/$LiClO_4$/SAP composite polymer electrolytes, a series of the CPEs with EO/Li = 6 and 0–10 wt.% of SAP (abbreviated as O6A*y*) were prepared and studied in the rest of this study.

Table 1
DSC thermal data of O*x* and O6A*y* electrolytes

Sample	T_g (°C)	T_m (°C)	ΔH (J g^{-1})	x_c%
O8	−26.7	43.4	18	12%
O7.5	−24.8	38.4	5	3%
O7	−22.2	–	–	–
O6	−18.2	–	–	–
O5	−20.7	83.4	–	–
O4	−23.1	84.7	–	–
O6A1	−25.7	–	–	–
O6A2	−30.2	–	–	–
O6A4	−24.5	–	–	–
O6A6	−23.0	–	–	–
O6A8	−22.8	–	–	–
O6A10	−22.5	–	–	–

In Fig. 4(b), the DSC thermograms of the O6A*y* samples show that with the addition of SAP, the crystallization of PEO remained suppressed. As the SAP loading was increased the T_g decreased first and then increased. The lowest T_g was obtained from O6A2. It is ascribed to the Lewis acid–base interactions of SAP with the lithium salt and PEO, which included the interactions of OH groups of SAP with the ClO_4^- ions and that with the ether oxygens [5,19]. These interactions reduced the interaction between the ether oxygens and the Li^+ ions, resulting in decrease of the cross-linking of the polymer chains via the Li^+ ions, consequently, decreased T_g of the polymer. The decrease of T_g reveals the increase in the flexibility of the PEO chains, facilitating the transport of Li^+ ions.

Fig. 5 shows the representative SEM/EDS surface images and the corresponding mappings of Si atoms of the O*x*A*y* CPEs. It is found out that the Si atoms were homogeneously distributed in the CPEs. Besides, no serious aggregation of SAP particles is observed in Fig. 5(a), suggesting that at lower contents, the SAP particles were well dispersed in the PEO/$LiClO_4$ matrix. However, as indicated in the circle, the granule size of the silica particles was significantly increased in Fig. 5(b) when the SAP content was increased to 8 wt.%, revealing an increase of aggregation that would reduce the effect of the filler on the property of the electrolyte; therefore, the CPE with SAP content higher than 8 wt.% was not studied in the rest of this study.

The TGA in Fig. 6 shows the weight lost of the polymer electrolytes below 200 °C. The small weight loss around 100 °C is ascribed to the evaporation of the water absorbed. Although the losses above 100 °C may be attributed to the solvent remained, they are all less than 4%, indicating that polymer electrolytes were basically solvent-free and thermally stable up to 200 °C. The enlarged plot in the inlet shows that the weight losses of O6A*y* in the temperature range were all less than that of O6 due to the presence of SAP.

3.3. FT-IR and ^{7}Li MAS NMR spectroscopy

Fig. 7 shows the FT-IR spectra of the O*x* and O6A*y* polymer electrolyte systems. The characteristic stretching vibrations of the C–O–C are observed as a triplet peak at about 1150, 1120, and 1060 cm^{-1}. The triplet absorption was broadened when $LiClO_4$ was added into the PEO matrix, suggesting the formation of the cross-linking complex through the interaction of the lithium ions and the ether oxygen [36]. However, the peak became sharper when SAP was dispersed in the electrolyte as found in Fig. 7(b) for O6A*y*. The result is ascribed to the existence of the Lewis acid–base interactions between the O atoms of silica and the Li^+ ions, resulting in reduction of the interactions between the Li^+ and the ether oxygen. This is consistent with the DSC and XRD results discussed above.

On the other hand, the change of the peak of ClO_4^- stretching vibration in the range of 650–600 cm^{-1} has been used to provide the information of the degree of salt dissociation in the

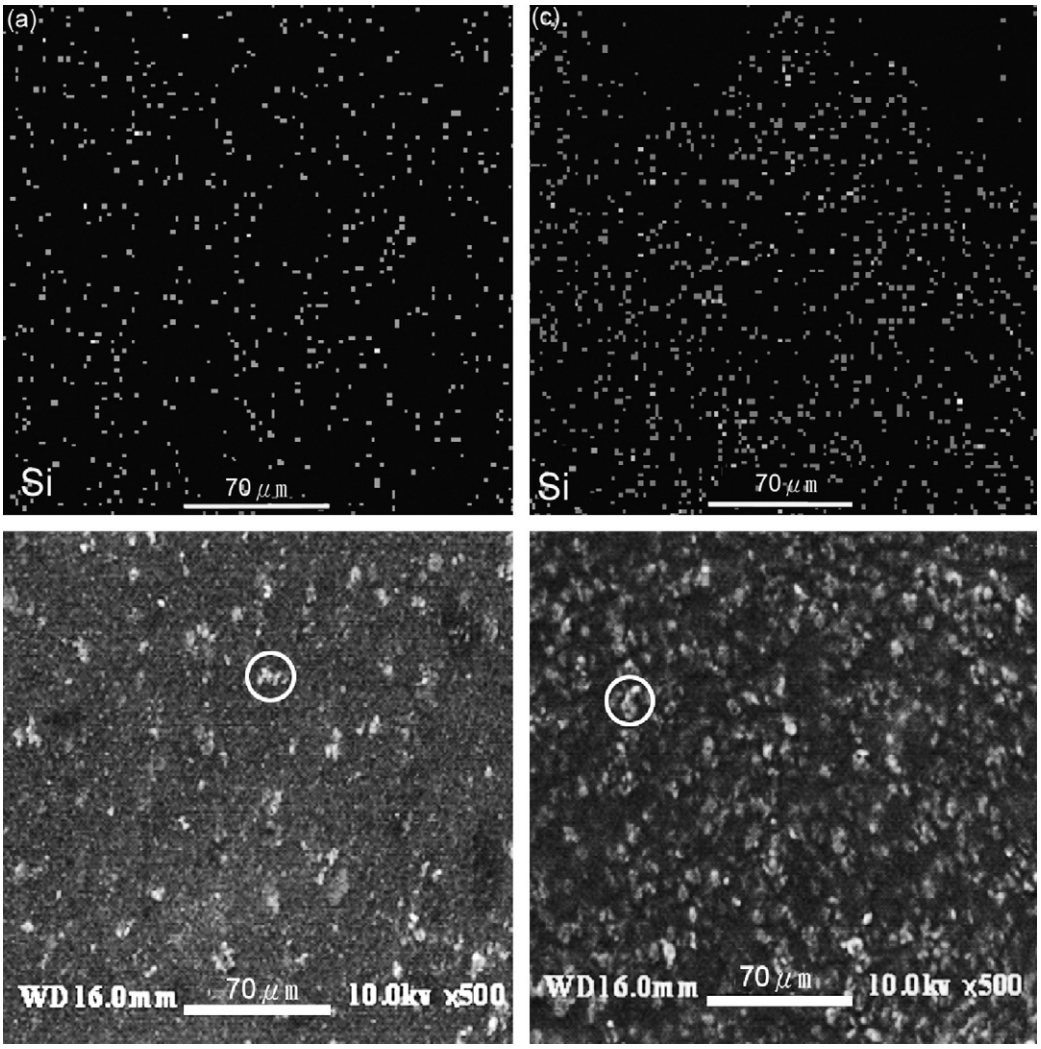

Fig. 5. SEM micrographs and Si mapping of (a) O6A1 and (b) O6A8.

$LiClO_4$-based electrolytes [20]. Fig. 8 shows the typical spectra with deconvoluted absorptions of the ClO_4^- stretching vibrations for O*x* and O6A*y* and the corresponding peak area ratios of the vibration peaks are summarized in Table 2. As reported previously [37], the peaks at ~635 and ~623 cm^{-1} are attributed to the ion-pair and the free ClO_4^-, respectively. It is noticed that for O*x* system the area ratio of the free ClO_4^- peak was higher than 80% when the EO/Li ratio was higher than 6, but significantly decreased when the EO/Li ratio was lower than 6, indicating that the percentage of salt dissociation was decreased as the salt concentration was too high due

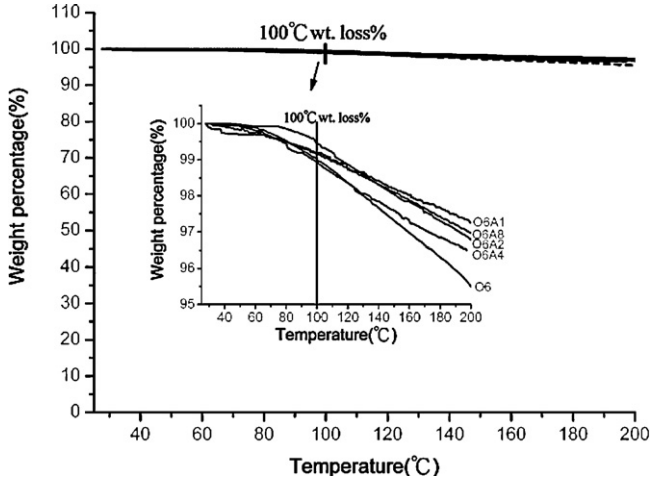

Fig. 6. TGA thermograms of O6A*y*.

Table 2
FT-IR peak positions and percentage of free ClO_4^- for O*x* and O6A*y* electrolytes

Sample	Free ClO_4^-		Bonded ClO_4^-	
	Wavenumber (cm^{-1})	(%)[a]	Wavenumber (cm^{-1})	(%)
O4	625	53	635	47
O5	623	70	633	30
O6	624	80	634	20
O7	623	81	633	19
O7.5	623	82	633	18
O8	624	84	636	16
O6A1	625	85	636	15
O6A2	624	96	637	4
O6A4	625	88	636	12
O6A6	625	88	636	12
O6A8	625	84	637	16
O6A10	625	81	636	19

[a] The percentage of the free ClO_4^- measured from the area ratio of the deconvoluted ClO_4^- peaks.

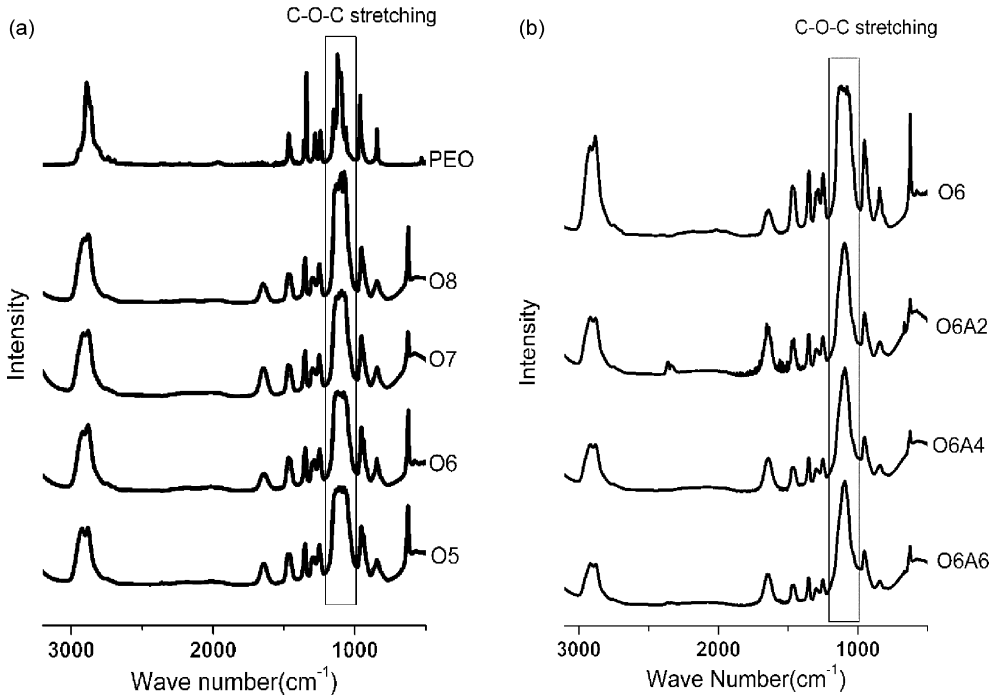

Fig. 7. FT-IR spectra of (a) O*x* and (b) O6A*y* electrolyte.

to lack of enough PEO chains for solvation with the Li^+ ions. However, the ratio of the free ClO_4^- was further increased with addition of SAP, implying an increase of the overall charge carriers. This is because of the formation of the extra interactions between the O atoms of SAP and Li^+ ions and between the surface OH groups of SAP and the ClO_4^- ions, enhancing the dissociation of the Li–ClO_4 ion-pairs. As high as 96% of free ClO_4^- was obtained from O6A2. This is attributed to the well distribution of the SAP particles with high surface area and porosity in the polymer electrolyte. Nevertheless, it decreased as the SAP content was exceeded 2 wt.% due to reduction of the interactions between SAP and the salt caused by the higher aggregation of the SAP nanoparticles, resulting in reduction of the surface area. The result also implies that O6A2 provided the most charge carriers among the as-prepared polymer electrolytes, which could facilitate the ionic conductivity.

^{7}Li MAS NMR with high power proton decoupling was used to investigate the coordination around the lithium ions of the as-prepared PEO-based polymer electrolytes. Fig. 9 presents the typical peak fitting spectra of O*x* and O6A*y* samples and the corresponding data are summarized in Table 3. As shown in Fig. 9(a), for O*x* samples, the down-field peak observed is assigned to the Li^+ bonded with ClO_4^-, i.e. ion-pair, and the up-field peak is assigned to the Li^+ coordinated with PEO [12]. It is noticed that the ion-pair content increased with the increase of the $LiClO_4$ concentration. This agrees with the FT-IR results discussed above. Moreover, the smallest half-width found for O6 indicates that the Li^+ in O6 has highest Li^+ mobility among the O*x* samples. With the addition of SAP, two more resonances were observed in the deconvoluted peak fitting spectra, revealing that two more Li^+ environments were formed due to coordination with SAP. However, when the SAP content reached 8 wt.% these resonances disappeared as indicated in Table 3 for O6A8. This is ascribed to the severe aggregations occurred. Besides, the decrease of ion-pairs with increase of SAP agrees with the results found from the FT-IR spectra, and the smallest half-width was obtained from O6A2, revealing that the Li^+ ions in O6A2 had the highest mobility. The result suggests that compared to that in

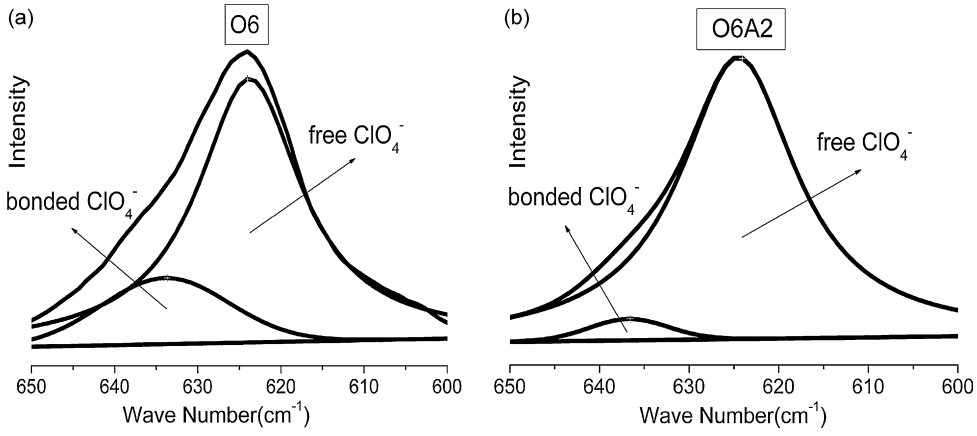

Fig. 8. FT-IR peak fitting of ClO_4^- absorbance for (a) O*x* and (b) O6A*y* electrolytes.

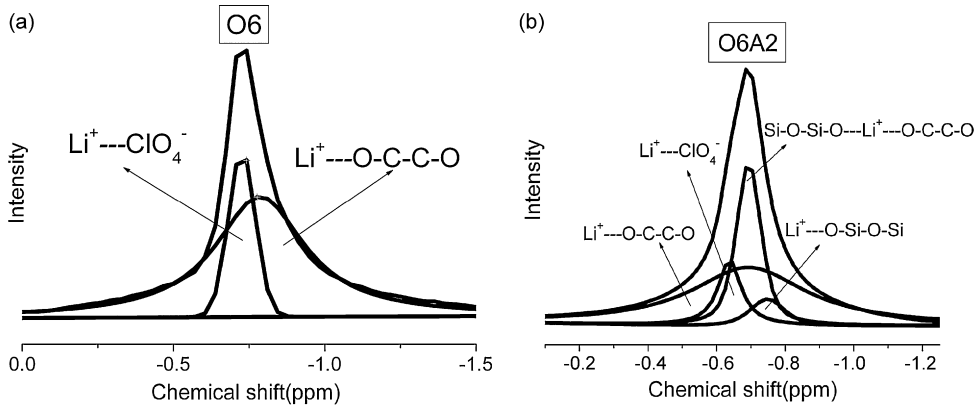

Fig. 9. Solid-state ^{7}Li MAS NMR peak fitting of (a) O*x* and (b) O6A*y* electrolyte series.

Table 3
^{7}Li NMR data of O*x* and O6A*y*

Sample	O8	O6	O5	O6A1	O6A2	O6A4	O6A8
Chemical shift (ppm)	−0.610	−0.714	−0.614	−0.752	−0.693	−0693	−0.594
$Li^+\cdots ClO_4^-$							
Chemical shift (ppm)	−0.64	−0.74	−0.63	−0.71	−0.64	−0.70	−0.57
Area ratio (%)	19	23	48	9	7	11	21
$Li^+\cdots O–C–C–O$							
Chemical shift (ppm)	−0.67	−0.78	−0.70	−0.81	−0.69	−0.83	−0.65
Area ratio (%)	81	77	52	58	50	55	63
$O–C–C–O\cdots Li^+\cdots O–Si–O–Si$							
Chemical shift (ppm)	–	–	–	−0.78	−0.68	−0.78	−0.61
Area ratio (%)	–	–	–	19	28	25	16
$Si–O–Si–O\cdots Li^+\cdots O–Si–O–Si$							
Chemical shift (ppm)	–	–	–	−0.75	−0.67	−0.73	–
Area ratio (%)	–	–	–	14	15	9	–
Half-width (ppm)	0.21	0.17	0.18	0.18	0.14	0.22	0.18

O6, the Li^+ ions should have extra conductive pathways in the CPE and O6A2 should have the highest ionic conductivity in the CPE system.

3.4. Ionic conductivity and Li^+ transference number

The bulk resistances, R_b, of the as-prepared polymer electrolytes were obtained from the ac impedance measurements as described in the previous work [38] and listed in Table 4. The ionic conductivities were then calculated with the thickness (L) and the surface area (A^*) of the specimen according to the following formula:

$$\sigma = \frac{L}{R_b A^*}$$

As can be seen in Table 4, the room temperature ionic conductivity of O*x* increased with increasing the lithium salt loading up to OE/Li = 6 then decreased. This is similar to the results reported and is ascribed to the combination effect of the degree of crystallinity and the ratio of the salt dissociation [39]. On the other hand, for O6A*y* system, the ionic conductivity increased with increasing SAP loading up to O6A2 then decreased as the SAP loading was further increased. The highest enhancement obtained from O6A2 is ascribed to the combination of the well dispersion of SAP with large surface area and porosity, amorphous structure of PEO, decrease of T_g and increase of charge carriers. The best conductivities at 30 °C for O*x* and O6A*y* systems were obtained from O6 (2.37×10^{-5} S cm^{-1}) and O6A2 (7.09×10^{-5} S cm^{-1}), respectively, indicating that with addition of 2 wt.% of SAP the conductivity of O6 was enhanced about threefold.

Fig. 10 shows the temperature dependence of the ionic conductivity for O*x* and O6A*y* systems. It is observed that the conductivities of all the samples increased steadily with increasing temperature in the range of 30–80 °C. Above 60 °C, the conductivity of O6A2 reached 10^{-4} S cm^{-1}, which is in the range for commercial applications. The linear plots reveal that the ionic conductivities of the samples are approximated to the Arrhenius equation in the temperature range [39]. This is unlike what is usually observed for most of the traditional amorphous solid polymer electrolytes, in which the ion conduction follows the VTF equation and the conduction

Table 4
Ionic conductivities and activation energies of O*x* and O6A*y* electrolytes[a]

Sample	R_b (Ω) 30 °C	L (mm)	σ (S cm^{-1}) 30 °C	E_a
O8	354	0.063	1.01×10^{-5}	27.82
O7.5	214	0.063	1.67×10^{-5}	26.10
O7	165	0.063	2.16×10^{-5}	24.04
O6	151	0.063	2.37×10^{-5}	23.98
O5	305	0.063	1.17×10^{-5}	24.59
O6A1	64	0.064	5.72×10^{-5}	15.20
O6A2	50	0.062	7.09×10^{-5}	14.95
O6A4	57	0.061	6.06×10^{-5}	19.71
O6A6	91	0.063	3.94×10^{-5}	25.13
O6A8	166	0.065	2.22×10^{-5}	25.90

[a] Surface area of the specimen = 1.76 cm^2.

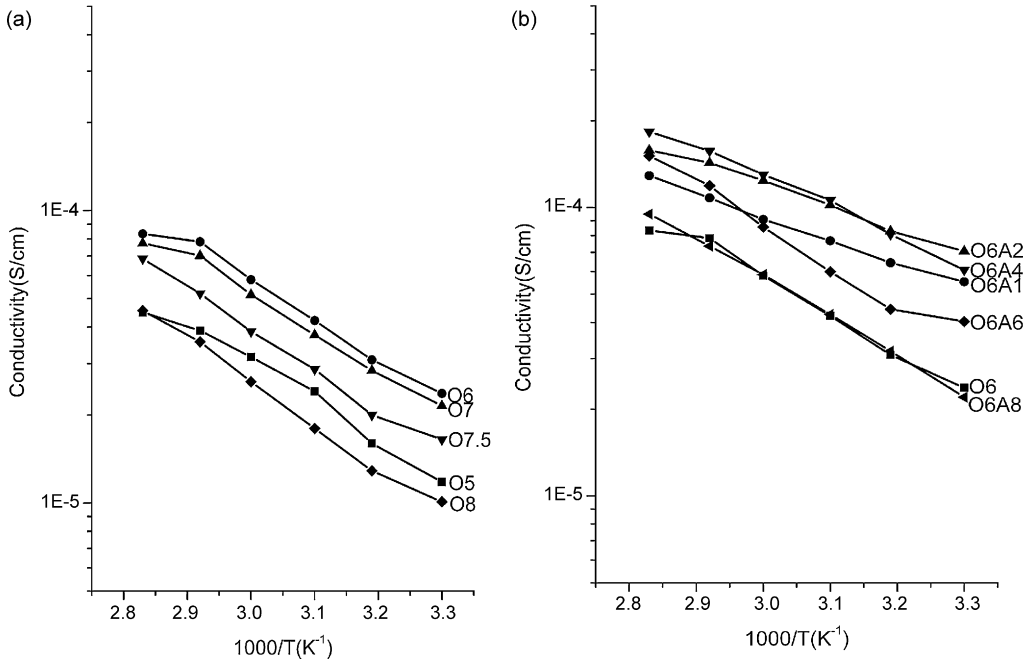

Fig. 10. Arrhenius plots of (a) O*x* and (b) O6A*y* electrolyte series.

mechanism is believed to involve the segmental motion of the polymer. In addition, as listed in Table 4, the E_a values obtained from these linear plots indicate that the ions can be activated more easily and transport faster in the as-prepared CPEs, O6A*x*, between 30 and 80 °C than in the corresponding SPE, O6, due to the presence of SAP. This reveals that the mobile charge carriers moved more freely in the polymer electrolyte with SAP than that without SAP. This is attributed not only to the amorphous structure of the CPE but also to the high surface area, interconnected pores and high porosity of SAP, which provided more Lewis active sites, shorter path and free volume for transporting the charge carriers.

As is known, a higher t^+ is anticipated to ensure the battery working at higher current density and better working efficiency. Therefore, the lithium ion transference numbers (t^+) of O6 and O6A*y* samples were measured as described in Section 2 to evaluate the contribution of the Li^+ species to the overall conductivity of the electrolyte. The original data of the electrochemical measurements of the Li/CPE/Li cells are summarized in Table 5. The corresponding t^+ was then calculated using the following equation [28,29]:

$$t^+ = \frac{I_s(\Delta V - I_0 R_0)}{I_0(\Delta V - I_s R_s)}$$

I_0 is the initial current, I_s the steady-state current, R_0 the initial interfacial resistance, R_s the steady-state interfacial resistance, and ΔV is the dc voltage applied.

As listed in Table 5, a low t^+ value (0.22) was obtained for the polymer solid electrolyte, O6, which is similar to the values (~0.2) reported [2]. However, the t^+ value was enhanced profoundly after addition of SAP, and as high as 0.69 was obtained for O6A2. This is attributed to the increase of fraction of the free Li^+ ions as well as the increase of transporting sites caused by the high surface area, shortening of the Li^+ ion transport path induced by the interconnected pores and increase of the free volume provided by the high porosity of SAP.

Table 5
The electrochemical data and transference numbers of O*x* and O6A*y* electrolytes

Sample	R_0 (Ω)	R_s (Ω)	I_0 (μA)	I_s (μA)	t^+
O6	260	345	10.7	2.45	0.22
O6A1	181	163	3.63	1.64	0.45
O6A2	163	190	1.41	0.94	0.67
O6A4	236	232	7.82	4.68	0.59
O6A8	266	299	9.93	3.28	0.32

4. Conclusions

A series of CPE composed of PEO, $LiClO_4$, with/without the as-prepared silica aerogel powder (SAP), have been studied as a function of both salt and SAP contents. The DSC investigations revealed that the polymer electrolytes without SAP (O*x*) with EO/Li = 6 and 7, O6 and O7, and the corresponding composite polymer electrolytes of O6 with 1–8 wt.% of SAP filler, O6A*y*, were all amorphous. The ionic conductivities of the polymer electrolytes varied with the change of the EO/Li ratio and the SAP content. The highest conductivity of the PEO/$LiClO_4$ solid polymer electrolyte was obtained from O6. Addition of the interconnected mesoporous SAP with high surface area and high porosity significantly increased the polymer segmental motion, fraction of free lithium ions, extra conductive pathway, transporting sites and free volume as well. Consequently, the mobility of the lithium ions was increased and the ionic conductivity and lithium ion transference number (t^+) of the CPE were significantly enhanced. The room temperature ionic conductivity and t^+ at 70 °C of O6A2 CPE were found to be 7.09×10^{-5} S cm^{-1} and 0.67, respectively. The values were both three times higher than that of the corresponding SPE, O6. These excellent properties made the as-prepared CPE a potential candidate to use in batteries.

Acknowledgments

The authors would like to thank National Science Council of Republic of China for supporting this research under contract no. 94-2113-M-033-010.

References

[1] D.E. Fenton, J.M. Parker, P.V. Wright, Polymer 14 (1973) 589.

[2] F. Croce, G.B. Appetecchi, L. Persi, B. Scrosati, Nature 394 (1998) 456–458.
[3] F.B. Dias, L. Plomp, J.B.J. Veldhuis, J. Power Sources 88 (2000) 169–191.
[4] J. Xi, X. Qiu, M. Cui, X. Tang, W. Zhu, L. Chen, J. Power Sources 156 (2006) 581–588.
[5] J.W. Kim, K.S. Ji, J.P. Lee, J.W. Park, J. Power Sources 119–121 (2003) 415–421.
[6] M.A.K.L. Dissanayake, P.A.R.D. Jayathilaka, R.S.P. Bokalawala, I. Albinsson, B.E. Mellander, J. Power Sources 119–121 (2003) 409–414.
[7] Y. Liu, J.Y. Lee, L. Hong, J. Appl. Polym. Sci. 89 (2003) 2815–2822.
[8] J. Xi, X. Qiu, X. Ma, M. Cui, J. Yang, X. Tang, W. Zhu, L. Chen, Solid State Ionics 176 (2005) 1249–1260.
[9] G. Sandĭı, K.A. Carrado, H. Joachin, W.Q. Lu, J. Prakash, J. Power Sources 119–121 (2003) 492–496.
[10] C.W. Nan, L. Fan, Y. Lin, Q. Cai, Phys. Rev. Lett. 91 (2003) 1–4, 266104.
[11] H.M. Kao, Y.Y. Tsai, S.W. Chao, Solid State Ionics 176 (2005) 1261–1270.
[12] M.J. Reddy, P.P. Chu, J. Power Sources 135 (2004) 1–8.
[13] Y. Tominaga, S. Asai, M. Sumita, S. Panero, B. Scrosati, J. Power Sources 146 (2005) 402–406.
[14] J. Xia, X. Qiua, W. Zhua, X. Tang, Microporous Mesoporous Mater. 88 (2006) 1–7.
[15] H.M. Kao, C.L. Chen, Angew. Chem. Int. Ed. 43 (2004) 980–984.
[16] H.M. Kao, S.W. Chao, P.C. Chang, Macromolecules 39 (2006) 1029–1040.
[17] F. Croce, R. Cuini, A. Matinelli, L. Persi, F. Ronci, B. Scrosati, J. Phys. Chem. B 103 (1999) 10632–10638.
[18] W. Wieczorek, P. Lipka, G. Zukowska, H. Wycislik, J. Phys. Chem. B 102 (1998) 6968–6974.
[19] E. Peled, D. Golodnitsky, G. Ardel, V. Eshkenazy, Electrochim. Acta 40 (1995) 2197–2204.
[20] S.H. Chung, Y. Wang, L. Persi, F. Croce, S.G. Greenbaum, B. Scrosati, E. Plichta, J. Power Sources 97–98 (2001) 644–648.
[21] P.A.R.D. Jayathilaka, M.A.K.L. Dissanayake, I. Albinsson, B.E. Mellander, Elctrochim. Acta 47 (2002) 3257–3268.
[22] M. Marcinek, A. Bac, P. Lipka, A. Zalewska, G. Zukowska, R. Borkowska, W. Wieczorek, J. Phys. Chem. B 104 (2000) 11088–11093.
[23] M.R. Ayers, A.J. Hunt, J. Non-Cryst. Solids 285 (2001) 123–127.
[24] L.W. Hrubesh, J. Non-Cryst. Solids 225 (1998) 335–342.
[25] J.S. Wilkes, M.J. Zaworotko, J. Chem. Soc., Chem. Commun. (1992) 965–967.
[26] S. Dai, Y.H. Ju, H.J. Gao, J.S. Lin, S.J. Pennycook, C.E. Barnes, Chem. Commun. (2000) 243–244.
[27] Y. Zhou, J.H. Schattka, M. Antonietti, Nano Lett. 4 (2004) 477–481.
[28] P.G. Bruce, C.A. Vincent, J. Electroanal. Chem. 225 (1987) 1–17.
[29] J. Evans, C.A. Vincent, P.G. Bruce, Polymer 28 (1987) 2324–2328.
[30] S. Dai, Y.H. Ju, H.J. Gao, J.S. Lin, S.J. Pennycook, C.E. Barnes, Chem. Commun. 3 (2000) 243–244.
[31] C.Y. Yuan, S. Dai, Y. Wei, Y.W. Chen-Yang, ACS Symp. Ser. 818 (2002) 106–113.
[32] K.W. Park, S.Y. Jeong, O.Y. Kwon, Appl. Clay Sci. 27 (2004) 21–27.
[33] D.J. Mead, R.M. Fuoss, J. Am. Chem. Soc. 62 (1940) 1720–1723.
[34] S. Gavalda, K.E. GuBBins, Y. Hanzawa, K. Kaneko, K.T. Thomson, Langmuir 18 (2002) 2141–2151.
[35] D. Zhao, Qi. Huo, Ji. Feng, B.F. Chmelka, G.D. Stucky, J. Am. Chem. Soc. 120 (1998) 6024–6036.
[36] M. Salomon, M. Xu, E.M. Eyring, S. Petrucci, J. Phys. Chem. 98 (1994) 8234–8244.
[37] H.W. Chen, C.Y. Chiu, F.C. Chang, J. Phys. Chem. B 40 (2002) 1342–1353.
[38] Y.W. Chen-Yang, J.J. Huang, F.H. Chang, Macromolecules 30 (1997) 3825–3831.
[39] P.P. Chu, M.J. Reddy, J. Tsai, J. Phys. Chem. B 42 (2004) 3866–3875.